SUPPORTING INFORMATION

Multifunctional and Recollectable Carbon Nanotube Ponytails for Water Purification

Haitao Wang,[1,†] Hanyu Ma,[1,†] Wen Zheng,[2] Dingding An,[2,*] and Chongzheng Na[1,*]

[1]Department of Civil and Environmental Engineering and Earth Sciences,

University of Notre Dame, Notre Dame, IN 46556, USA

[2]Department of Microbiology and Immunobiology,

Harvard Medical School, Boston, MA 02115, USA

*Corresponding author: chongzheng.na@gmail.com, dingding_an@hms.harvard.edu

[†]These authors contributed equally.

Table of Contents

1. Structures of Layered Double Hydroxide and Layer Double Oxide Discs

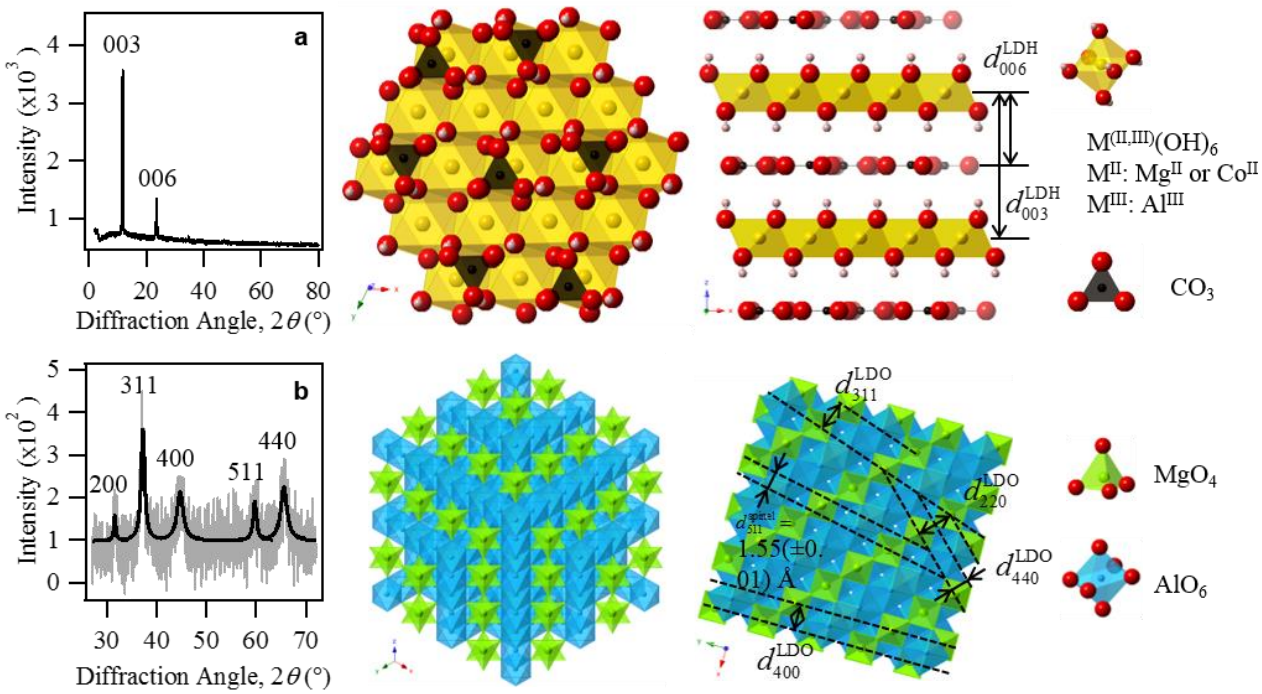

Figure S1. Powder X-ray diffraction patterns of (a) layered double hydroxide (LDH) and (b) layered double oxide discs. The patterns confirm that LDH has a hydrotalcite structure and LDO has a spinel structure.

2. Control of Physical Dimensions of Carbon Nanotube Ponytails

The physical dimensions of carbon nanotube ponytails (CNPs) can be tuned by varying parameters such as synthesis time and cobalt doping. As illustrated in Figure S2a, we have investigated the control of the radius of CNP cross section *r*, CNP's half-length *l*, carbon nanotube (CNT) outer diameter *d*, and CNT wall number *n*. We measured *r*, *l*, *d*, and *n* from transmission electron micrographs of samples made under 4 different synthesis conditions. A set of measurements were then used to create a histogram, which was fit to a Gaussian function to obtain estimates of the average value and standard deviation. An example for how the average and standard deviation of *r* was obtained is shown in Figure S2b.

The radius of CNP cross section, *r*, was controlled by varying the time used to synthesize LDH through co-precipitation of Al, Mg, and Co hydroxides. An example is shown in Figure S2c with 13% Co in the original reactive solution (i.e., $\alpha = 13\%$). For synthesis that lasted less than 2 hours, we observed little LDH formation. With samples made between 2 and 4 hours, we observed a few measurable LDH discs but large amounts of small nuclei. We then observed numerous LDH discs with further increase of synthesis time. The size length of the discs, which would be the radius of CNPs once CNTs were grown, increased monotonically with increasing synthesis time. Based on these observations, we concluded that the synthesis of LDH was dominated by the nucleation phase before 4 hours and then transitioned to the growth phase after 4 hours.

We can model the growth of LDH by considering the rate-limiting step of co-precipitation, which is the hydrolysis of urea to carbonate:[1]

$$CO(NH_2)_2 \underset{k_2}{\overset{k_1}{\rightleftarrows}} NH_4^+ + OCN^- \qquad \text{(S1)}$$

$$OCN^- + 2H_2O \xrightarrow{k_3} NH_4^+ + CO_3^{2-} \qquad \text{(S2).}$$

These reactions are rate-limiting because carbonate is the intercalated anion that is required to fuse metal hydroxide sheets (cf. Figure S1e). Accordingly, kinetics of Reactions S1 and S2 can be expressed as follows:

$$\frac{d[\mathrm{CO(NH_2)_2}]}{dt} = -k_1[\mathrm{CO(NH_2)_2}] + k_2[\mathrm{NH_4^+}][\mathrm{OCN^-}] \qquad \text{(S3)}$$

$$\frac{d[\mathrm{OCN^-}]}{dt} = k_1[\mathrm{CO(NH_2)_2}] - k_2[\mathrm{NH_4^+}][\mathrm{OCN^-}] - k_3[\mathrm{OCN^-}] \qquad \text{(S4)}$$

$$\frac{d[\mathrm{CO_3^{2-}}]}{dt} = k_3[\mathrm{OCN^-}] \qquad \text{(S5).}$$

We can neglect $k_2[\mathrm{NH_4^+}][\mathrm{OCN^-}]$ in the above equations on the basis that the formation and growth of LDH discs are sinks of carbonate, which drive the overall reaction forward. As a result, $k_1[\mathrm{CO(NH_2)_2}] >> k_2[\mathrm{NH_4^+}][\mathrm{OCN^-}]$. We can further apply the pseudo steady state condition for the reaction intermediate cyanate,[2] which gives:

$$\frac{d[\mathrm{OCN^-}]}{dt} = k_1[\mathrm{CO(NH_2)_2}] - k_3[\mathrm{OCN^-}] = 0 \qquad \text{(S6).}$$

After simplification, Equation S3 becomes

$$\frac{d[\mathrm{CO(NH_2)_2}]}{dt} \approx -k_1[\mathrm{CO(NH_2)_2}] \qquad \text{(S7).}$$

Integrating Equation S7 gives:

$$[\mathrm{CO(NH_2)_2}] \approx u_0\left(1 - e^{-k_1 t}\right) \qquad \text{(S8),}$$

where u_0 is the initial urea concentration. Combining Equations S5, S6, and S8 gives:

$$\frac{d[\mathrm{CO_3^{2-}}]}{dt} = k_3[\mathrm{OCN^-}] \approx k_1[\mathrm{CO(NH_2)_2}] = k_1 u_0\left(1 - e^{-k_1 t}\right) \qquad \text{(S9).}$$

Integrating Equation S9 from time 0 to t gives:

$$[CO_3^{2-}] = u_0\left(k_1 t + e^{-k_1 t} - 1\right) \qquad \text{(S10)}.$$

If we assume all carbonate produced by urea hydrolysis is taken up by LDH growth immediately after formation, we have

$$[CO_3^{2-}]V = 3r^2\delta\eta N \qquad \text{(S11)}.$$

where V is the reactor volume, r is the side length of LDH hexagons, δ is the thickness of LDH hexagons, η is the molar concentration of carbonate in LDH, and N is the number of LDH hexagons. We further assume that δ and N are determined at the early stage of LDH formation (i.e., t < 10 hr) and thus are constants at the later growth stage. Combining Equations S10 and S11 gives:

$$r = A\left(k_1 t + e^{-k_1 t} - 1\right)^{\frac{1}{2}};\ A = \left(\frac{u_0 V}{3\delta\eta N}\right)^{\frac{1}{2}} \qquad \text{(S12)}.$$

The first term is a constant while the second term reveals the dependence on t. Using the measured values of r at $t \geq 10$ hr, we estimate k_1 = 0.37(±0.24) hr^{-1} from least-square regression. This value is consistent with the first-order rate constant of 0.147 hr^{-1} at circumneutral pH and 100 ^{o}C.[1] We also obtained A = 1.1(±0.4) μm. Using u_0 = 100 mmol L^{-1}, V = 100 mL, δ = 40(±16) nm, and η = 1.53 mol L^{-1} (for hydrotalcite), we estimate N = 4.5(±3.7) × 10^7, which suggests that there are approximately 10 to 100 million LDH disks in 100 mL of reaction solution. The fitted model, together with its 68.3% percentile confidence intervals, is shown in Figure S1c, which serves as a guideline to control the dimension of CNP cross section.

Different from synthesis time in co-precipitation that varies the size of LDH discs, the variation of cobalt molar percentage in the reactive solution did not, however, change the size of LDH discs (and consequently the size of CNP cross section), as shown in Figure S2d. This is consistent with the fact that Co, Mg, and Al are interchangeable in the LDH structure (cf. Figure S1e). When the Co percentage was varied, the total amount of Co, Mg, and Al was kept constant.

For growing CNTs on LDO derived from LDH using chemical vapor deposition, as reaction time increased, most growth occurred in the first 15 min. After that, growth quickly reached a steady state. These results are shown in Figure S2e with CNT growth expressed as the percentage of the steady-state mass. The observation that CNTs cease to grow after certain time in CVD can be attributed to blockage or poisoning of metal catalysts,[3-4] which are Co nanoparticles in our synthesis system.

Using 15 min as the growth time for CVD, we further investigated the change of CNP half-length *l*, CNT outer diameter *d*, and CNT wall number *n* as shown in Figure S2f, g, and h. Both *d* and *n* increased with increasing Co percentage whereas *l* increased for $\alpha < 20\%$ and then decreased for $\alpha > 20\%$. The variations of *l*, *d*, and *n* with α can be rationalized by considering the increase of size of Co nanoparticles as α increases because Co nanoparticles were the catalysts from which CNTs were grown. As shown in Figure S2i, the nominal diameter of Co nanoparticles, d_{Co}, increased with increasing α monotonically. Mass balance dictates that d_{Co} and α are related as follows:

$$d_{Co} = \rho\, \alpha^{1/3} \qquad \text{(S13)},$$

where ρ is a constant determined by the dimensions of Co hollow spheres. We estimated that ρ = 4.0(±0.3) using least-square regression (R^2 = 0.97 with an intercept of 1.0(±0.8) being essentially zero). The monotonic increases of *d* and *n* with increasing α can be attributed to the increase of d_{Co} with α because larger Co nanoparticles will catalyze the growth of CNTs with greater diameter and wall number. The positive correlation is also applicable to *l* and α at $\alpha < 20\%$. However, at $\alpha >$ 20% increases of *d* and *n* dramatically increase the need of carbon mass. The expansion in the radial direction redirects carbon atoms that used to extend CNTs' length to increasing their diameters, which results in the decrease of *l* with increasing α for $\alpha > 20\%$.

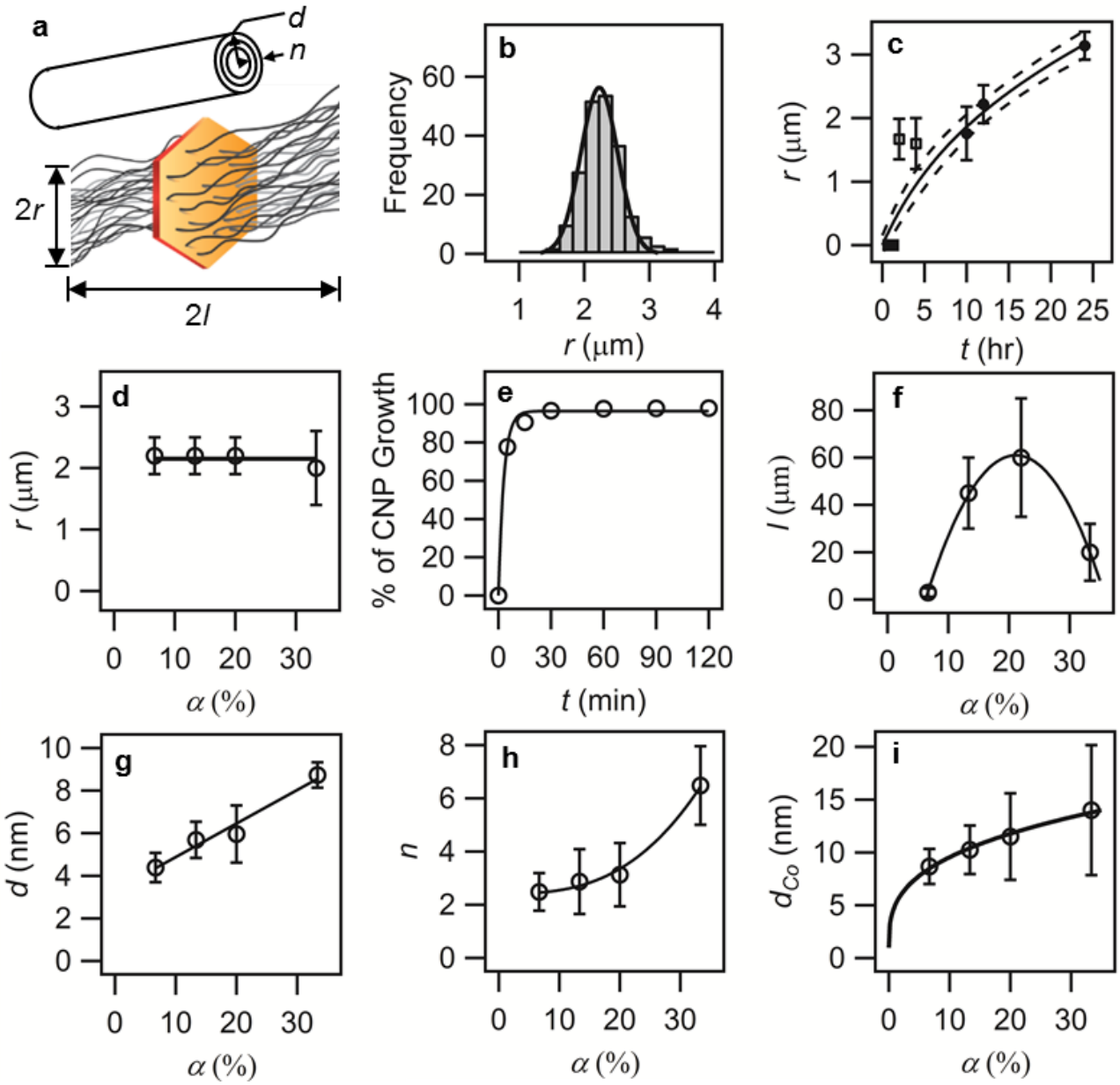

Figure S2. Control of physical dimensions of carbon nanotube ponytails (CNPs) by varying synthesis time and cobalt doping (α = [Co]/([Co] + [Mg] + [Al])). (a) Diagram showing the physical parameters including radius of CNP cross section r, CNP half-length l, carbon nanotube (CNT) outer diameter d, and CNT wall number n. (b) Example histogram for estimating r with a Gaussian fit. (c) Increase of r with reaction time t (α = 13%). The solid curve represents the regression of r and t to Equation S12 using data at $t \geq 10$ hr (solid circles). The dashed curves mark the confidence interval corresponding to one standard deviation (68.3%). The horizontal solid bar at $r = 0$ and extending from $t = 0$ to 2 hr represents our observation of little LDH discs nor nuclei at the early stage of synthesis. (d) Invariance of r with increasing α. (e) Growth of CNPs with increasing synthesis time for chemical vapor deposition, expressed as the percentage of CNTs in CNPs. (f, g, h) Changes of l, d, and n with increasing α fitted with polynomials. (i) Nominal diameter of Co nanoparticles on LDO with fit to Equation S13.

3. Surface Hydrophobicity of Unbounded Carbon Nanotubes Determined Using X-Ray Photoelectron Spectroscopy

Surfaces of carbon nanotubes consisting of graphene sheets are intrinsically hydrophobic. When surfaces are functionalized with oxygen-containing groups such as –COOH, –OH, and –O–, they become hydrophilic. With surfaces being hydrophobic or hydrophilic, CNPs and CNTs can have different affinities with water, which in turn affect their settling behavior in water. To exclude the possibility that surface wettability had affected settling of CNTs and CNPs in water, we performed X-ray photoelectron spectroscopy (XPS; PHI 5000 VersaProbe) measurements. In our measurements, we used the monochromatized Al Kα line (1486.6 eV) as incident X-ray. The standard deviation of peak position was determined to be approximately 0.05 eV.

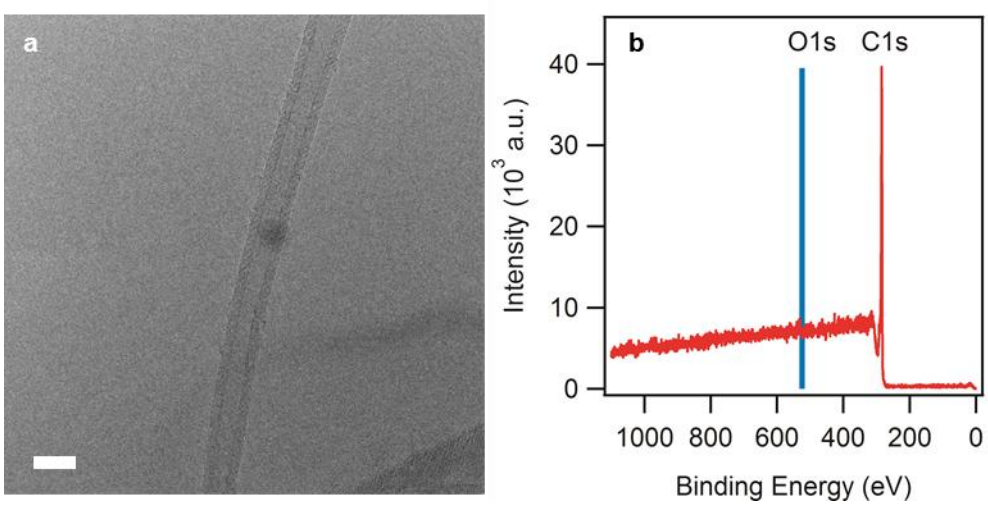

Figure S3. Transmission electron microscopy (a) and X-ray photoelectron spectrum (b) of unbound carbon nanotubes. Scale bar: 10 nm.

As shown in Figure 2e in the main text and Figure S3 above, both surfaces showed strong the C_{1S} peak at 284.6 eV,[5] which were consist with a graphene surface with minimal functionalization. The position for the O_{1S} peak had a reading within uncertainty of the baselines.

According to the width of the baseline, we determined that the O content of both samples were below 1.5%. According to one report,[6] when surface O content was below 3%, carbon nanotubes were always neutral and hydrophobic from pH 5 to 9. According to another report,[7] when the O content was below 6%, carbon nanotubes were superhydrophobic. Based on our measurements and these reports, we concluded both CNPs and CNTs used in our experiments had hydrophobic surfaces. Therefore, both samples had little affinity with water and their settling in water should be affected by surface hydrophobicity similarly. In other words, any difference in settling between CNPs and CNTs must be attributed to factors other than difference in surface properties. As we stated in the main text, we believe that difference in settling is due to the difference in size between CNPs and CNTs.

4. Results of Least-Square Regressions in Figures 5 and 6

Table S1. Results of Linear Regressions in Figure 5a

pH	C_o (mg L^{-1})	X (g L^{-1})	q_e (mg g^{-1})	k_a (g mg^{-1} min^{-1})	R^2	t for q/q_e = 95%
8	30	0.67	46(±1)	0.017(±0.003)	0.999	24.3(±4.3)
6	30					
6	60		84(±2)	0.0028(±0.0002)	0.996	80.8(±6.1)
6	200		148(±5)	0.00036(±0.00003)	0.995	357(±32)

Table S2. Results of Linear Regression in Figure 5b

pH	C_o (mg L^{-1})	X (g L^{-1})	q_{max} (mg g^{-1})	K (L mg^{-1})	R^2
4 – 10	60 – 200	0.5 – 1	150(±9)	0.42(±0.42)	0.98

Table S3. Results of Linear Regressions in Figure 5c

n	$q_{o,n}$ (mg g^{-1})	$t_{o,n}$ (min)	X (g L^{-1})	$C_{e,n}$ (mg L^{-1})	$k_{d,n}$ (L mg^{-1} min^{-1})	R^2
1	98	0	0.67	29.8(±0.1)	0.063(±0.002)	1.000
2	53	120		6.11(±0.02)	0.052(±0.005)	1.000
3	44	240		3.49(±0.06)	0.037(±0.003)	0.998

Table S4. Results of Linear Regressions in Figure 5d

C_o (mg L^{-1})	X (g L^{-1})	$d\theta/dN$ (%)	R^2
80	0.4	-1.9(±0.4)	0.95

Table S5. Results of Linear Regressions in Figure 5e

Cycle	$\theta_{(8\ min)}$ (%)	$d\theta/dt$ (% min^{-1})	R^2
1	92	10(±2)	0.97
2	48	6.9(±0.9)	0.98
3	4	0.6(±0.2)	0.87

Table S6. Results of Linear Regression in Figure 6b

pH	N_o (CFUs mL^{-1})	X (g L^{-1})	q_{max} (CFUs g^{-1})	K (L g^{-1})	R^2
7	1.3×10^5	0 – 0.2	$2.3(\pm0.2) \times 10^9$	0.2 (±0.2)	0.97

5. Quantification of Carbon Nanotubes and Carbon Nanotube Ponytails in Aqueous Suspensions Using UV/vis Spectrometry

Carbon nanotubes and carbon nanotube ponytails are good absorbents of visible light, as indicated by their black color and shown by the intensive absorption of light from 400 to 700 nm using a Cary 100 UV/vis spectrophotometer, as shown in Figure S4a. The light-absorbing property was utilized to quantify concentrations of CNTs and CNPs suspended in water by sonication (5 min). We selected 500 nm as the wavelength in our measurement although light with other wavelength between 400 and 700 nm should also work.

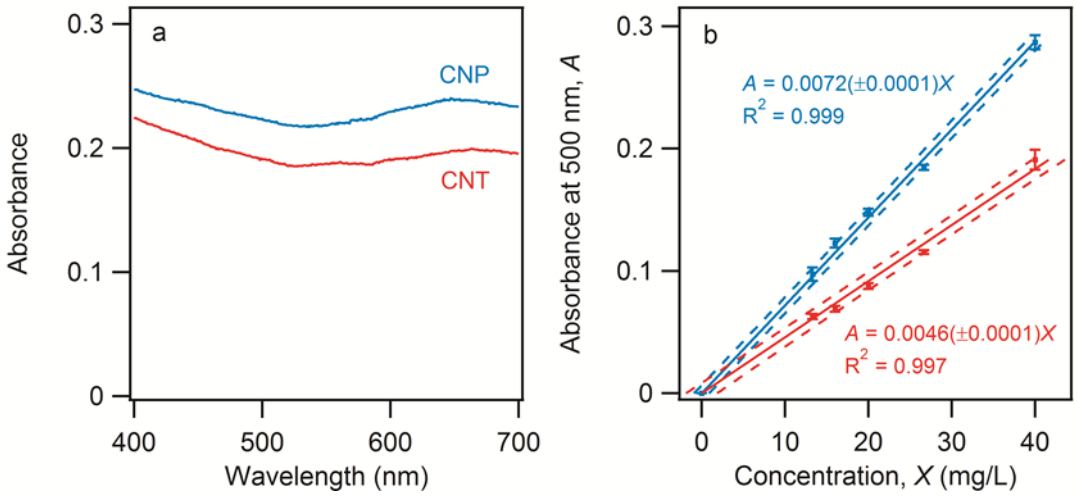

Figure S4. Visible spectra (a) and the absorbance-concentration relationships (b) for carbon nanotubes (CNTs) and carbon nanotube ponytails (CNPs) dispersed in water. Concentrations of CNTs and CNPs in *a* are 40 and 30 mg/L, respectively. The solid lines are least-square regressions of experimental data to Equation S14. The dashed lines bracket one standard deviation of prediction.

To make a calibration curve that can relate light absorbance at 500 nm to the concentration of CNTs or CNPs suspended in water, we mixed different amounts of CNTs or CNPs with 50 mL DI water under sonication for 5 minutes. To obtain the accurate mass of CNTs or CNPs, the samples were freeze-dried before weighing. As shown in Figure S4b, absorbance and

concentration has a linear relationship for both CNTs and CNPs. We modeled the linear relationship using Beer's law:

$$A = \varepsilon X L \qquad \text{(S14)},$$

where $A = \log(I/I_0)$ is absorbance, I_0 is the intensity of the incident light, I is the intensity of the transmitted light, ε is the extinction coefficient, X is the concentration, and L is the length of the light path (L = 1 cm in our experiments). According to the slopes of the absorbance-concentration linear relationships, we estimate the specific extinction coefficients of water-dispersed CNT and CNP to be ε_{CNT} = 4.6(±0.1) cm^2 mg^{-1} and ε_{CNP} = 7.2(±0.1) cm^2 mg^{-1}. Both estimates are consistent with the values of extinction coefficients for well-dispersed CNTs.[8-11]

Average settling velocity v can be obtained from the change of X with t according to the following equation:

$$\frac{VdX}{dt} = \alpha v X \qquad \text{(S15)},$$

where V is the volume of the suspension and α is cross-section area of the settling vial. This equation relates the flux of CNTs or CNPs settled out of the suspension with the flux at the bottom of the suspension. Integration of Equation S15 gives

$$\ln\frac{X}{X_o} = -\frac{\alpha}{V}vt = -\frac{v}{h}t \qquad \text{(S16)},$$

where h is the height of the suspension.

6. Quantification of *p*-Nitrophenol Reduction Using UV/vis Spectrometry

The reduction of PNP by sodium borohydride ($NaBH_4$; SB) to *p*-aminophenol (PAP) is a well-studied reaction:[12]

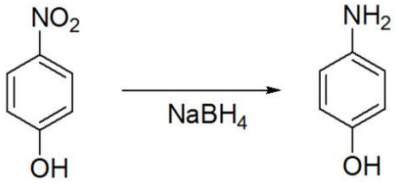

(S17).

The hydrogenation reaction is greatly promoted by the presence of catalysts such as Pd nanoparticles (PdNPs), whose surface facilitates the generation of hydrogen. The procession of this reaction can be readily detected by naked eyes as the yellow color of PNP fades away with time in the presence of excess SB. As shown in Figure S5a, the absorption spectrum of PNP in $NaBH_4$ peaked at 400 nm, due to the formation of *p*-nitrophenolate from dissociation ($pK_a = 7.2$).[13] In comparison, PAP absorbs minimal light from 325 to 600 nm.[14-15] This suggests that the absorbance at 400 nm can be used to quantify the PNP concentration according to Beer's law (cf. Equation S14), as shown by the calibration curve in Figure S5b. Measuring PNP concentration periodically as time passes provides measurements of the kinetics of Reaction S17.

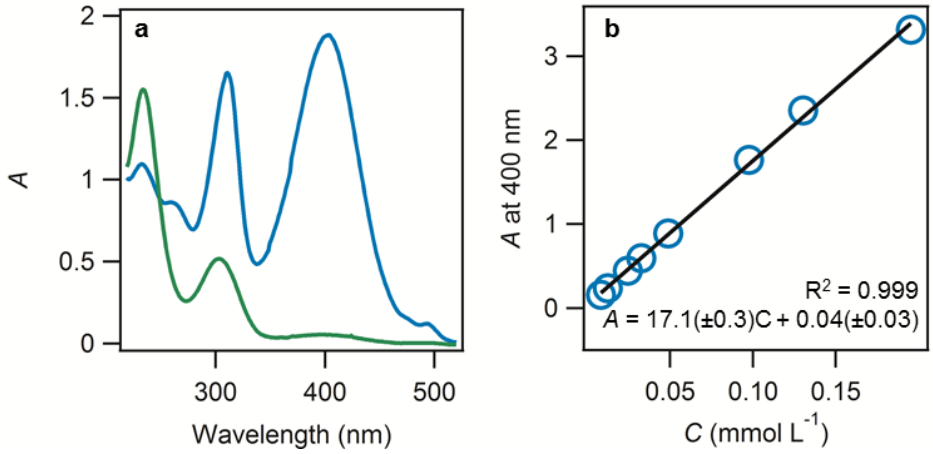

Figure S5. (a) UV/vis spectra of *p*-nitrophenol (cyan) and *p*-aminophenol (green) and (b) the absorbance-concentration relationship used for *p*-nitrophenol quantification.

References

1. Warner, R. C., The Kinetics of the Hydrolysis of Urea and of Arginine. *J. Biol. Chem.* **1942**, *142*, 705-723.
2. Fogler, H. S., *Elements of Chemical Reaction Engineering*. Prentice Hall PTR: Upper Saddle River, NJ, 2000.
3. Yasuda, S.; Futaba, D. N.; Yamada, T.; Satou, J.; Shibuya, A.; Takai, H.; Arakawa, K.; Yumura, M.; Hata, K., Improved and Large Area Single-Walled Carbon Nanotube Forest Growth by Controlling the Gas Flow Direction. *ACS Nano* **2009**, *3*, 4164-4170.
4. Reilly, P. T. A.; Whitten, W. B., The Role of Free Radical Condensates in the Production of Carbon Nanotubes During the Hydrocarbon CVD Process. *Carbon* **2006**, *44*, 1653-1660.
5. Okpalugo, T. I. T.; Papakonstantinou, P.; Murphy, H.; McLaughlin, J.; Brown, N. M. D., High Resolution Xps Characterization of Chemical Functionalised Mwcnts and Swcnts. *Carbon* **2005**, *43*, 153-161.
6. Smith, B.; Wepasnick, K.; Schrote, K. E.; Cho, H.-H.; Ball, W. P.; Fairbrother, D. H., Influence of Surface Oxides on the Colloidal Stability of Multi-Walled Carbon Nanotubes: A Structure−Property Relationship. *Langmuir* **2009**, *25*, 9767-9776.
7. Aria, A. I. Control of Wettability of Carbon Nanotube Array by Reversible Dry Oxidation for Superhydrophobic Coating and Supercapacitor Applications. Ph.D., California Institute of Technology, Ann Arbor, 2013.
8. Bahr, J. L.; Mickelson, E. T.; Bronikowski, M. J.; Smalley, R. E.; Tour, J. M., Dissolution of Small Diameter Single-Wall Carbon Nanotubes in Organic Solvents? *Chem. Commun.* **2001**, 193-194.
9. Roldo, M.; Power, K.; Smith, J. R.; Cox, P. A.; Papagelis, K.; Bouropoulos, N.; Fatouros, D. G., *N*-Octyl-*O*-Sulfate Chitosan Stabilises Single Wall Carbon Nanotubes in Aqueous Media and Bestows Biocompatibility. *Nanoscale* **2009**, *1*, 366-373.
10. Liu, Y. Q.; Yao, Z. L.; Adronov, A., Functionalization of Single-Walled Carbon Nanotubes with Well-Defined Polymers by Radical Coupling. *Macromolecules* **2005**, *38*, 1172-1179.
11. Zhou, B.; Lin, Y.; Li, H. P.; Huang, W. J.; Connell, J. W.; Allard, L. F.; Sun, Y. P., Absorptivity of Functionalized Single-Walled Carbon Nanotubes in Solution. *J. Phys. Chem. B* **2003**, *107*, 13588-13592.
12. Pradhan, N.; Pal, A.; Pal, T., Catalytic Reduction of Aromatic Nitro Compounds by Coinage Metal Nanoparticles. *Langmuir* **2001**, *17*, 1800-1802.
13. Liu, J.; Qin, G.; Raveendran, P.; Ikushima, Y., Facile "Green" Synthesis, Characterization, and Catalytic Function of β-D-Glucose-Stabilized Au Nanocrystals. *Chem. Eur. J.* **2006**, *12*, 2131-2138.
14. Dotzauer, D. M.; Bhattacharjee, S.; Wen, Y.; Bruening, M. L., Nanoparticle-Containing Membranes for the Catalytic Reduction of Nitroaromatic Compounds. *Langmuir* **2009**, *25*, 1865-1871.
15. Ballarin, B.; Cassani, M. C.; Tonelli, D.; Boanini, E.; Albonetti, S.; Blosi, M.; Gazzano, M., Gold Nanoparticle-Containing Membranes from in Situ Reduction of a Gold(III)−Aminoethylimidazolium Aurate Salt. *J. Phys. Chem. C* **2010**, *114*, 9693-9701.